Chapter 8

Neutrino oscillations

In the case of a non-vanishing rest mass of the neutrino, the weak and mass eigenstates are not necessarily identical, a fact well known in the quark sector where both types of states are connected by the CKM matrix (see section 3.3.2). This allows for the phenomenon of neutrino oscillations, a kind of flavor oscillation which is already known in other particle systems. It can be described by pure quantum field theory. Oscillations are observable as long as the neutrino wave packets form a coherent superposition of states. Such oscillations among the different neutrino flavors do not conserve individual flavor lepton numbers, only total lepton number. We start with the most general case first, before turning to the more common two- and three-flavor scenarios. For additional literature see [Bil78, Bil87, Kay81, Kay89, Boe92, Kim93, Gri96, Gro97, Sch97, Bil99, Lip99, Giu07, Dor08, Akh09].

8.1 General formalism

The following discussion is based on simplified arguments, nevertheless, resulting in correct equations. A sophisticated derivation can be done within quantum field theory; see [Kay81, Gri96, Akh09].

Let us assume that there is an arbitrary number of n orthonormal eigenstates. The n flavor eigenstates $|\nu_\alpha\rangle$ with $\langle\nu_\beta|\nu_\alpha\rangle = \delta_{\alpha\beta}$ are connected to the n mass eigenstates $|\nu_i\rangle$ with $\langle\nu_i|\nu_j\rangle = \delta_{ij}$ via a unitary mixing matrix U:

$$|\nu_\alpha\rangle = \sum_i U_{\alpha i}|\nu_i\rangle \qquad |\nu_i\rangle = \sum_\alpha (U^\dagger)_{i\alpha}|\nu_\alpha\rangle = \sum_\alpha U^*_{\alpha i}|\nu_\alpha\rangle \tag{8.1}$$

with

$$U^\dagger U = 1 \qquad \sum_i U_{\alpha i}U^*_{\beta i} = \delta_{\alpha\beta} \qquad \sum_\alpha U_{\alpha i}U^*_{\alpha j} = \delta_{ij}. \tag{8.2}$$

In the case of antineutrinos, i.e. $U_{\alpha i}$ has to be replaced by $U^*_{\alpha i}$:

$$|\bar\nu_\alpha\rangle = \sum_i U^*_{\alpha i}|\bar\nu_i\rangle. \tag{8.3}$$

The number of parameters in an $n \times n$ unitary matrix is n^2. The $2n-1$ relative phases of the $2n$ neutrino states can be fixed in such a way that $(n-1)^2$ independent parameters remain. It is convenient to write them as $\frac{1}{2}n(n-1)$ weak mixing angles of an n-dimensional rotational matrix together with $\frac{1}{2}(n-1)(n-2)$ CP-violating phases.

The mass eigenstates $|\nu_i\rangle$ are stationary states and show a time dependence according to

$$|\nu_i(x,t)\rangle = \mathrm{e}^{-\mathrm{i}E_i t}|\nu_i(x,0)\rangle \tag{8.4}$$

assuming neutrinos with momentum p emitted by a source positioned at $x = 0$ $(t = 0)$

$$|\nu_i(x,0)\rangle = \mathrm{e}^{\mathrm{i}px}|\nu_i\rangle \tag{8.5}$$

and being relativistic

$$E_i = \sqrt{m_i^2 + p_i^2} \simeq p_i + \frac{m_i^2}{2p_i} \simeq E + \frac{m_i^2}{2E} \tag{8.6}$$

for $p \gg m_i$ and $E \approx p$ as neutrino energy. Assume that the difference in mass between two neutrino states with different mass $\Delta m_{ij}^2 = m_i^2 - m_j^2$ cannot be resolved. Then the flavor neutrino is a coherent superposition of neutrino states with definite mass.[1] Neutrinos are produced and detected as flavor states. Therefore, neutrinos with flavor $|\nu_\alpha\rangle$ emitted by a source at $t = 0$ develop with time into a state

$$|\nu(x,t)\rangle = \sum_i U_{\alpha i}\mathrm{e}^{-\mathrm{i}E_i t}|\nu_i\rangle = \sum_{i,\beta} U_{\alpha i}U^*_{\beta i}\mathrm{e}^{\mathrm{i}px}\mathrm{e}^{-\mathrm{i}E_i t}|\nu_\beta\rangle. \tag{8.7}$$

Different neutrino masses imply that the phase factor in (8.7) is different. This means that the flavor content of the final state differs from the initial one. At macroscopic distances this effect can be large in spite of small differences in neutrino masses. The time-dependent transition amplitude for a flavor conversion $\nu_\alpha \to \nu_\beta$ is then given by

$$A(\alpha \to \beta)(t) = \langle \nu_\beta|\nu(x,t)\rangle = \sum_i U^*_{\beta i}U_{\alpha i}\mathrm{e}^{\mathrm{i}px}\mathrm{e}^{-\mathrm{i}E_i t}. \tag{8.8}$$

Using (8.6) this can be written as

$$\begin{aligned} A(\alpha \to \beta)(t) = \langle \nu_\beta|\nu(x,t)\rangle &= \sum_i U^*_{\beta i}U_{\alpha i}\exp\left(-\mathrm{i}\frac{m_i^2}{2}\frac{L}{E}\right) \\ &= A(\alpha \to \beta)(L) \end{aligned} \tag{8.9}$$

with $L = x = ct$ being the distance between source and detector. In an analogous way, the amplitude for antineutrino transitions can be derived ((8.8)):

$$A(\bar{\alpha} \to \bar{\beta})(t) = \sum_i U_{\beta i}U^*_{\alpha i}\mathrm{e}^{-\mathrm{i}E_i t}. \tag{8.10}$$

[1] This is identical to the kaon system. The states K^0 and $\bar{\mathrm{K}}^0$ are states of definite strangeness which are related to K^0_S and K^0_L as states with definite masses and widths.

The transition probability P can be obtained from the transition amplitude A:

$$P(\alpha \to \beta)(t) = |A(\alpha \to \beta)|^2 = \sum_i \sum_j U_{\alpha i} U^*_{\alpha j} U^*_{\beta i} U_{\beta j} \mathrm{e}^{-\mathrm{i}(E_i - E_j)t}$$
$$= \sum_i |U_{\alpha i} U^*_{\beta i}|^2 + 2\,\mathrm{Re} \sum_{j>i} U_{\alpha i} U^*_{\alpha j} U^*_{\beta i} U_{\beta j} \exp\left(-\mathrm{i}\frac{\Delta m^2_{ij}}{2}\right) \frac{L}{E} \tag{8.11}$$

with

$$\Delta m^2_{ij} = m^2_i - m^2_j. \tag{8.12}$$

The second term in (8.11) describes the time- (or spatial-) dependent neutrino oscillations. The first one is an average transition probability, which also can be written as

$$\langle P_{\alpha\to\beta} \rangle = \sum_i |U_{\alpha i} U^*_{\beta i}|^2 = \sum_i |U^*_{\alpha i} U_{\beta i}|^2 = \langle P_{\beta\to\alpha} \rangle. \tag{8.13}$$

Using CP invariance ($U_{\alpha i}$ real), this can be simplified to

$$P(\alpha \to \beta)(t) = \sum_i U^2_{\alpha i} U^2_{\beta i} + 2 \sum_{j>i} U_{\alpha i} U_{\alpha j} U_{\beta i} U_{\beta j} \cos\left(\frac{\Delta m^2_{ij}}{2} \frac{L}{E}\right)$$
$$= \delta_{\alpha\beta} - 4 \sum_{j>i} U_{\alpha i} U_{\alpha j} U_{\beta i} U_{\beta j} \sin^2\left(\frac{\Delta m^2_{ij}}{4} \frac{L}{E}\right). \tag{8.14}$$

Evidently, the probability of finding the original flavor is given by

$$P(\alpha \to \alpha) = 1 - \sum_{\alpha \neq \beta} P(\alpha \to \beta). \tag{8.15}$$

As can be seen from (8.11) there will be oscillatory behaviour as long as at least one neutrino mass eigenstate is different from zero and if there is a mixing (non-diagonal terms in U) among the flavors. In addition, the observation of oscillations allows no absolute mass measurement; oscillations are sensitive to only Δm^2. Last but not least, neutrino masses should not be exactly degenerated. Another important feature is the dependence of the oscillation probability on L/E. Majorana phases as described in Chapter 7 are unobservable in oscillations because the form given in (7.28) and implemented in (8.11) shows that the diagonal matrix containing the phases always results in the identity matrix [Bil80]. The same results for oscillation probabilities are also obtained by performing a more sophisticated quantum field theoretical treatment using wave packets [Kay81, Gri96, Akh09].

The result can also be obtained from very general arguments [Gro97, Lip99], which show that such flavor oscillations are completely determined by the propagation dynamics and the boundary condition that the probability of observing the wrong flavor at the position of the source at any time must vanish. The

propagation in free space for each state is given in (8.4). The expansion of the neutrino wavefunction in energy eigenstates is

$$\psi = \int g(E)\,\mathrm{d}E\,\mathrm{e}^{-\mathrm{i}Et}\sum_{i=1}^{3} c_i \mathrm{e}^{\mathrm{i}px}|\nu_i\rangle \tag{8.16}$$

with the energy-independent coefficients c_i. The function $g(E)$ describing the exact form of the energy wavepacket is irrelevant at this stage. Each energy eigenstate has three terms, one for each mass eigenstate, if three generations are assumed. The boundary condition for creating a ν_e and only a ν_e at the source (or at $t = 0$) then requires

$$\sum_{i=1}^{3} c_i\langle\nu_i|\nu_\mu\rangle = \sum_{i=1}^{3} c_i\langle\nu_i|\nu_\tau\rangle = 0. \tag{8.17}$$

The momentum of each of the three components is determined by the energy and the neutrino masses. The propagation of this energy eigenstate, the relative phases of its three mass components and its flavor mixture at the detector are completely determined by the energy–momentum kinematics of the three mass eigenstates and lead to the same oscillation formula as described before.

8.2 CP and T violation in neutrino oscillations

Comparison of (8.8) with (8.10) yields a relation between neutrino and antineutrino transitions:

$$A(\bar{\alpha} \to \bar{\beta})(t) = A(\alpha \to \beta)(t) \neq A(\beta \to \alpha)(t). \tag{8.18}$$

This relation is a direct consequence of the CPT theorem. CP violation manifests itself if the oscillation probabilities of $\nu_\alpha \to \nu_\beta$ are different from its CP conjugate process $\bar{\nu}_\alpha \to \bar{\nu}_\beta$. So an observable would be

$$\Delta P^{CP}_{\alpha\beta} = P(\nu_\alpha \to \nu_\beta) - P(\bar{\nu}_\alpha \to \bar{\nu}_\beta) \neq 0 \qquad \alpha \neq \beta. \tag{8.19}$$

This has to be done with the proposed neutrino superbeams and neutrino factories (see section 8.10). Similarly, T violation can be tested if the probabilities of $\nu_\alpha \to \nu_\beta$ are different from the T conjugate process $\nu_\beta \to \nu_\alpha$. Here, the observable is

$$\Delta P^{T}_{\alpha\beta} = P(\nu_\alpha \to \nu_\beta) - P(\nu_\beta \to \nu_\alpha) \neq 0 \qquad \alpha \neq \beta. \tag{8.20}$$

If CPT conservation holds, which is the case for neutrino oscillations in vacuum, violation of T is equivalent to violation of CP. Using U_{MNS} it can be shown explicitly that in vacuum $\Delta P^{CP}_{\alpha\beta}$ and $\Delta P^{T}_{\alpha\beta}$ are equal and given by

$$\begin{aligned}\Delta P^{CP}_{\alpha\beta} &= \Delta P^{T}_{\alpha\beta} \\ &= -16 J_{\alpha\beta} \sin\left(\frac{\Delta m^2_{12}}{4E}L\right)\sin\left(\frac{\Delta m^2_{23}}{4E}L\right)\sin\left(\frac{\Delta m^2_{13}}{4E}L\right)\end{aligned} \tag{8.21}$$

where

$$J_{\alpha\beta} \equiv \mathrm{Im}[U_{\alpha 1} U^*_{\alpha 2} U^*_{\beta 1} U_{\beta 2}] = \pm c_{12} s_{12} c_{23} s_{23} c^2_{13} s_{13} \sin\delta \tag{8.22}$$

corresponds to the Jarlskog invariant as in the quark sector, and the $+(-)$ sign denoting cyclic (anticyclic) permutation of $(\alpha, \beta) = (\mathrm{e}, \mu), (\mu, \tau), (\tau, \mathrm{e})$. Note that for CP or T violation effects to be present, all the angles must be nonzero and, therefore, three-flavor mixing is essential. To be a bit more specific we now consider the case of two-flavor oscillations.

8.3 Oscillations with two neutrino flavors

This is still by far the most common case used in data analysis which is justified in the next chapters. However, planned precision measurements require a three-flavor analysis. In this case the relation between the neutrino states is described by one mixing angle θ and one mass difference, for example $\Delta m^2 = m^2_2 - m^2_1$. The unitary transformation (8.1) is analogous to the Cabibbo matrix in the quark sector and given by (taking ν_e and ν_μ):

$$\begin{pmatrix} \nu_e \\ \nu_\mu \end{pmatrix} = \begin{pmatrix} \cos\theta & \sin\theta \\ -\sin\theta & \cos\theta \end{pmatrix} \begin{pmatrix} \nu_1 \\ \nu_2 \end{pmatrix}. \tag{8.23}$$

Using the formulae from the previous section, the corresponding two-flavor transition probability is given because there is no CP violating phase by

$$\begin{aligned} P(\nu_e \to \nu_\mu) = P(\nu_\mu \to \nu_e) = P(\bar\nu_e \to \bar\nu_\mu) = P(\bar\nu_\mu \to \bar\nu_e) \\ = \sin^2 2\theta \times \sin^2 \frac{\Delta m^2}{4} \times \frac{L}{E} = 1 - P(\nu_e \to \nu_e). \end{aligned} \tag{8.24}$$

This formula explicitly shows that oscillations occur only if both θ and Δm^2 are non-vanishing. All two-flavor oscillations probabilities can be characterized by these two quantities because $P(\nu_\alpha \to \nu_\beta) = P(\nu_\beta \to \nu_\alpha)$. The phase factor can be rewritten as

$$\frac{E_i - E_j}{\hbar} t = \frac{1}{2\hbar c} \Delta m^2_{ij} \frac{L}{E} = 2.534 \frac{\Delta m^2_{ij}}{\mathrm{eV}^2} \frac{L/m}{E/\mathrm{MeV}} \tag{8.25}$$

where in the last step some practical units were used. The oscillatory term can then be expressed as

$$\begin{aligned} \sin^2 \left(\frac{\Delta m^2_{ij}}{4} \frac{L}{E} \right) &= \sin^2 \pi \frac{L}{L_0} \\ \text{with } L_0 &= 4\pi\hbar c \frac{E}{\Delta m^2} = 2.48 \frac{E/\mathrm{MeV}}{\Delta m^2/\mathrm{eV}^2} m. \end{aligned} \tag{8.26}$$

In the last step the oscillation length L_0, describing the period of one full oscillation cycle, is introduced (Figure 8.1). It becomes larger with higher energies and smaller Δm^2. The mixing angle $\sin^2 2\theta$ determines the amplitude of the oscillation while

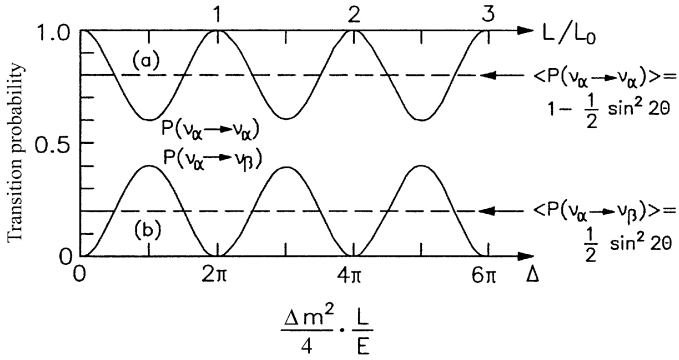

Figure 8.1. Example of neutrino oscillations in the two-flavor scheme: upper curve, $P(\nu_\alpha \rightarrow \nu_\alpha)$ (disappearance); lower curve, $P(\nu_\alpha \rightarrow \nu_\beta)$ (appearance) as a function of $L/L_0 = \Delta m^2/4\pi$ for $\sin^2 2\theta = 0.4$. The dashed lines show the average oscillation probabilities (after [Sch97]). With kind permission from Springer Science + Business Media.

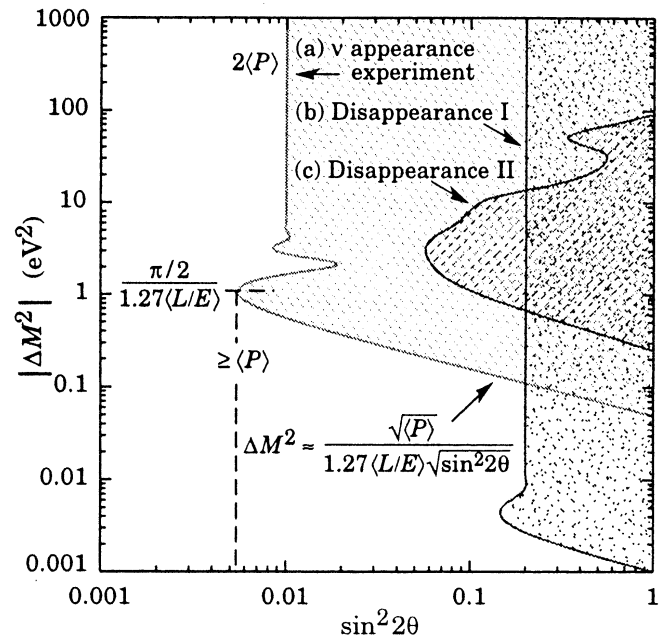

Figure 8.2. Standard double logarithmic plot of Δm^2 *versus* $\sin^2 2\theta$. The excluded parameter ranges of hypothetical appearance and disappearance experiments are shown. At low Δm^2 the experiment loses sensitivity being too close to the source, so the oscillation barely develops. This implies a slope of -2 until one reaches maximal sensitivity in the first oscillation maximum. At very high Δm^2 the oscillation itself can no longer be observed, only an average transition probability (after [GRO00]).

Δm^2 influences the oscillation length. Both unknown parameters are typically drawn in a double logarithmic plot as shown in Figure 8.2. The relative phase of the two neutrino states at a position x is (see (8.16))

$$\delta\phi(x) = (p_1 - p_2)x + \frac{(p_1^2 - p_2^2)}{(p_1 + p_2)}x = \frac{\Delta m^2}{(p_1 + p_2)}x. \tag{8.27}$$

Since the neutrino mass difference is small compared to all momenta $|m_1 - m_2| \ll p \equiv (1/2)(p_1 + p_2)$, this can be rewritten in first order in Δm^2 as

$$\delta\phi(x) = \frac{\Delta m^2}{2p}x \tag{8.28}$$

identical to (8.24) with $x = L$ and $p = E$.

8.4 The case for three flavors

A more realistic scenario to consider is that of three known neutrino flavors, which will be addressed by the next generation of precision neutrino experiments. The mixing matrix $U_{\rm MNS}$ is given in Chapter 5. Note that now more Δm^2 quantities are involved both in magnitude and sign: although in a two-flavor oscillation in vacuum the sign does not enter, in three-flavor oscillation, which includes both matter effects (see section 8.9) and CP violation, the signs of the Δm^2 quantities enter and can, in principle, be measured. In the absence of any matter effect, the probability is given by

$$\begin{aligned} P(\nu_\alpha \to \nu_\beta) = \delta_{\alpha\beta} &- 4\sum_{i>j=1}^{3} \mathrm{Re}(K_{\alpha\beta,ij}) \sin^2\left(\frac{\Delta m^2_{ij} L}{4E}\right) \\ &+ 4\sum_{i>j=1}^{3} \mathrm{Im}(K_{\alpha\beta,ij}) \sin\left(\frac{\Delta m^2_{ij} L}{4E}\right) \cos\left(\frac{\Delta m^2_{ij} L}{4E}\right) \end{aligned} \tag{8.29}$$

where

$$K_{\alpha\beta,ij} = U_{\alpha i} U^*_{\beta i} U^*_{\alpha j} U_{\beta j}. \tag{8.30}$$

The general formulae in the three-flavor scenario are quite complex; therefore, the following assumption is made: in most cases only one mass scale is relevant, i.e., $\Delta m^2_{\rm atm} \sim$ few $\times\ 10^{-3}$ eV^2, which is discussed in more detail in Chapter 9. Furthermore, one possible neutrino mass spectrum such as the hierarchical one is taken:

$$\Delta m^2_{21} = \Delta m^2_{\rm sol} \ll \Delta m^2_{31} \approx \Delta m^2_{32} = \Delta m^2_{\rm atm}. \tag{8.31}$$

Then the expressions for the specific oscillation transitions are:

$$\begin{aligned} P(\nu_\mu \to \nu_\tau) &= 4|U_{33}|^2 |U_{23}|^2 \sin^2\left(\frac{\Delta m^2_{\rm atm} L}{4E}\right) \\ &= \sin^2(2\theta_{23}) \cos^4(\theta_{13}) \sin^2\left(\frac{\Delta m^2_{\rm atm} L}{4E}\right) \end{aligned} \tag{8.32}$$

$$P(\nu_e \to \nu_\mu) = 4|U_{13}|^2|U_{23}|^2 \sin^2\left(\frac{\Delta m^2_{\rm atm} L}{4E}\right)$$
$$= \sin^2(2\theta_{13}) \sin^2(\theta_{23}) \sin^2\left(\frac{\Delta m^2_{\rm atm} L}{4E}\right) \quad (8.33)$$

$$P(\nu_e \to \nu_\tau) = 4|U_{33}|^2|U_{13}|^2 \sin^2\left(\frac{\Delta m^2_{\rm atm} L}{4E}\right)$$
$$= \sin^2(2\theta_{13}) \cos^2(\theta_{23}) \sin^2\left(\frac{\Delta m^2_{\rm atm} L}{4E}\right). \quad (8.34)$$

8.5 Experimental considerations

The search for neutrino oscillations can be performed in two different ways—an appearance or disappearance mode. In the latter case one explores whether less than the expected number of neutrinos of a produced flavor arrive at a detector or whether the spectral shape changes if observed at various distances from a source. This method is not able to determine the new neutrino flavor. An appearance experiment searches for possible new flavors, which do not exist in the original beam or produce an enhancement of an existing neutrino flavor. The identification of the various flavors relies on the detection of the corresponding charged lepton produced in their charged current interactions

$$\nu_l + \mathrm{N} \to l^- + \mathrm{X} \qquad \text{with } \mathrm{l} \equiv \mathrm{e}, \mu, \tau \quad (8.35)$$

where X denotes the hadronic final state.

Several neutrino sources can be used to search for oscillations which will be discussed in this and the following chapters more extensively. The most important ones are:

- nuclear power plants ($\bar{\nu}_e$),
- accelerators (ν_e, ν_μ, $\bar{\nu}_e$, $\bar{\nu}_\mu$),
- the atmosphere (ν_e, ν_μ, $\bar{\nu}_e$, $\bar{\nu}_\mu$) and
- the Sun (ν_e).

which shows that the various mentioned sources sometimes cannot probe each other; i.e., high-energy accelerators ($E \approx$ 1–100 GeV, $L \approx 1$ km) are not able to check the solar neutrino data ($E \approx 1$ MeV, $L \approx 10^8$ km). Equation (8.36) also defines the minimal Δm^2 which can be explored. Three cases have to be considered with respect to a possible observation of oscillations (Figure 8.3):

- $L/E \ll \frac{4}{\Delta m^2}$, i.e. $L \ll L_0$. Here, the experiment is too close to the source and the oscillations have no time to develop.
- $L/E \gtrsim \frac{4}{\Delta m^2}$, i.e. $L/E \gtrsim \frac{1}{\Delta m^2}$. This is a necessary condition to observe oscillations and it is the most sensitive region.

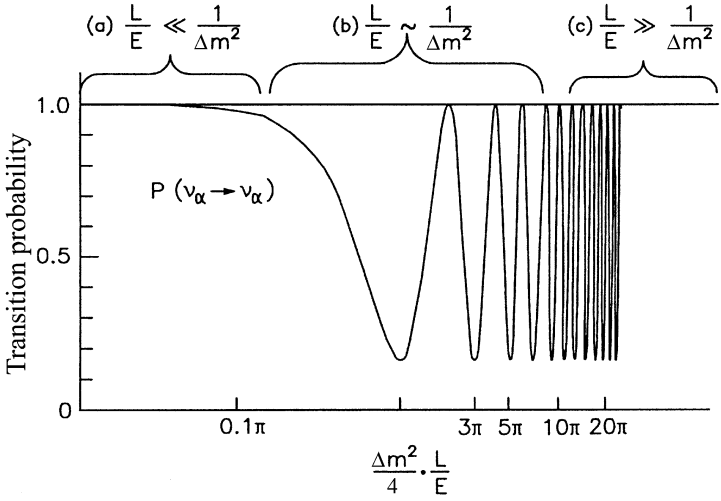

Figure 8.3. Logarithmic plot of the oscillation probability $P(\nu_\alpha \rightarrow \nu_\alpha)$ as a function of L/E for $\sin^2 2\theta = 0.83$. The brackets denote three possible cases: (a) no oscillations ($L/E \ll 1/\Delta m^2$); (b) maximal sensitivity to oscillations $L/E \approx 1/\Delta m^2$; and (c) only average oscillation measurement due to finite resolution for $L/E \gg 1/\Delta m^2$ (after [Sch97]). With kind permission from Springer Science + Business Media.

- $L/E \gg \frac{4}{\Delta m^2}$, i.e. $L \gg L_0$. Several oscillations have happened between the source and the detector. Normally, experiments do then measure L/E not precisely enough to resolve the oscillation pattern but measure only an average transition probability.

Thus, the part of the Δm^2–$\sin^2 2\theta$ parameter space explored depends on the ratio L/E. The most sensitive range of an experiment is at

$$\Delta m^2 \approx E/L. \tag{8.36}$$

Two more points which influence the experimental sensitivity to and the observation of oscillations have to be considered. First of all, L is often not well defined. This is the case when dealing with an extended source (Sun, atmosphere, decay tunnels). Alternatively, E might not be known exactly. This might be the case if the neutrino source has an energy spectrum $N(E)$ and E will not be measured in a detector. Last but not least, for some experiments there is no chance to vary L and/or E because it is fixed (e.g., in the case of the Sun); therefore, the explorable Δm^2 region is constrained by nature.

8.6 Nuclear reactor experiments

Nuclear reactors are the strongest terrestrial antineutrino source, coming from the β-decays of unstable neutron-rich products of ^{235}U, ^{238}U, ^{239}Pu and ^{241}Pu fission.

The average yield is about $6\bar{\nu}_e$/fission. The flux density is given by

$$\Phi_\nu = 1.5 \times 10^{12} \frac{P/\mathrm{MW}}{L^2/\mathrm{m}^2}\ \mathrm{cm}^{-2}\,\mathrm{s}^{-1} \tag{8.37}$$

where P is the thermal power (in MW) of the reactor and L (in m) is the distance from the reactor core. The total isotropic flux of emitted $\bar{\nu}_e$ is then ($F = 4\pi L^2$)

$$F\Phi_\nu = 1.9 \times 10^{17} \frac{P}{\mathrm{MW}}\ \mathrm{s}^{-1}. \tag{8.38}$$

Reactor experiments are disappearance experiments looking for $\bar{\nu}_e \to \bar{\nu}_X$, because the energy is far below the threshold for μ, τ production. The spectrum peaks around 2–3 MeV and extends up to about 8 MeV. Experiments typically try to measure the positron spectrum which can be deduced from the $\bar{\nu}_e$ spectrum and either compare it directly to the theoretical predictions or measure it at several distances from the reactor and search for spectral changes. Both types of experiments have been performed in the past. However, the first approach requires a detailed theoretical understanding of the fission processes as well as a good knowledge of the operational parameters of the reactor during a duty cycle which changes the relative contributions of the fission products.

The detection reaction used mostly is

$$\bar{\nu}_e + p \to \mathrm{e}^+ + \mathrm{n} \tag{8.39}$$

with an energy threshold of 1.806 MeV. The $\bar{\nu}_e$ energy can be obtained by measuring the positron energy spectrum as

$$E_{\bar{\nu}_e} = E_{e^+} + m_n - m_p = E_{e^+} + 1.293\ \mathrm{MeV} = T_{e^+} + 1.806\ \mathrm{MeV} \tag{8.40}$$

with T_{e^+} as kinetic energy of the positron and neglecting the small neutron recoil energy ($\approx$20 keV). The cross section for (8.39) is given by

$$\begin{aligned}\sigma(\bar{\nu}_e + p \to e^+ + n) &= \sigma(\nu_e + n \to e^- + p) \\ &= \frac{G_F^2 E_\nu^2}{\pi} |\cos\theta_c|^2 \left(1 + 3\left(\frac{g_A}{g_\nu}\right)^2\right) \\ &= 9.23 \times 10^{-42} \left(\frac{E_\nu}{10\ \mathrm{MeV}}\right)^2\ \mathrm{cm}^2. \end{aligned} \tag{8.41}$$

Normally, coincidence techniques are used for detection between the annihilation photons and the neutrons which diffuse and thermalize within 10–100 μs. The neutrons will be captured by (n, γ) reactions resulting in a second pulse of photons for detection.

Sometimes the reactions

$$\bar{\nu}_e + \mathrm{D} \to \mathrm{e}^+ + \mathrm{n} + \mathrm{n} \qquad (E_{\mathrm{Thr}} = 4.0\ \mathrm{MeV}) \qquad (\mathrm{CC}) \tag{8.42}$$

$$\bar{\nu}_e + \mathrm{D} \to \bar{\nu}_e + \mathrm{p} + \mathrm{n} \qquad (E_{\mathrm{Thr}} = 2.2\ \mathrm{MeV}) \qquad (\mathrm{NC}) \tag{8.43}$$

Table 8.1. List of finished 'short-baseline' ($\leq$ 300 m) reactor experiments. The power of the reactors and the distance of the experiments with respect to the reactor are given.

Reactor	Thermal power [MW]	Distance [m]
ILL-Grenoble (F)	57	8.75
Bugey (F)	2800	13.6, 18.3
Rovno (USSR)	1400	18.0, 25.0
Savannah River (USA)	2300	18.5, 23.8
Gösgen (CH)	2800	37.9, 45.9, 64.7
Krasnojarsk (Russia)	?	57.0, 57.6, 231.4
Bugey III (F)	2800	15.0, 40.0, 95.0

were used.

The main backgrounds in reactor neutrino experiments originate from uncorrelated cosmic-ray hits in coincidence with natural radioactivity and correlated events from cosmic-ray muons and induced neutrons [Boe00, Bem02].

8.6.1 Experimental status

Several reactor experiments have been performed in the past (see table 8.1). All these experiments had a fiducial mass of less than 0.5 t and the distance to the reactor was never more than 250 m. Two new reactor experiments performed recently were CHOOZ and Palo Verde, which will be discussed in a little more detail. Both were motivated by the fact that the ν_e might participate in the atmospheric neutrino anomaly, discussed in more detail in Chapter 9. The fact, that the testable Δm^2 region is between 10^{-2}–10^{-3} eV^2 requires a distance of about 1 km to the reactors.

8.6.1.1 CHOOZ

The CHOOZ experiment in France [Apo98, Apo99, Apo03] was performed between April 1997 and July 1998. It had some advantages with respect to previous experiments. The detector was located 1115 m and 998 m away from two 4.2 GW reactors, more than a factor four in comparison to previous experiments. In addition, the detector was located underground with a shielding of 300 mwe (mwe = meter water equivalent). The shielding power of overburden is normally expressed as height of a water column with equivalent shielding, reducing the background due to atmospheric muons by a factor of 300. This allowed the construction of a homogeneous detector (Figure 8.4). The main target was about 4.8 t and hence is much larger than those used before. It consisted of a specially developed scintillator loaded with 0.1% Gd within an acrylic vessel. This inner detector was surrounded by an additional detector containing 17 t of scintillator without Gd and 90 t of scintillator as an outer veto. The signal is the detection of the annihilation photons in coincidence with n-capture on Gd, the latter producing gammas with a total sum of

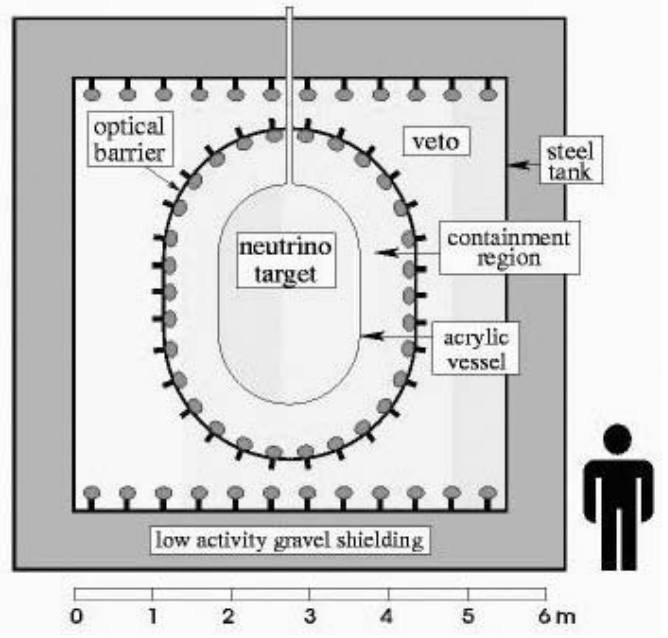

Figure 8.4. Schematic drawing of the CHOOZ detector (from [Apo98]). © 1998 Reprinted with permission from Elsevier.

8 MeV. The average neutron capture time was about 30.5 μs. The published positron spectrum [Apo98] is shown in Figure 8.5 and shows no hints for oscillation. The measured energy averaged ratio between expected and observed events is

$$R = 1.01 \pm 2.8\%(\text{stat.}) \pm 2.7\%(\text{sys.}). \tag{8.44}$$

This result is in perfect agreement with the absence of any oscillations, leading to the exclusion plot shown in Figure 8.6. This limits any mixing angle with electrons (also θ_{13}) to

$$\sin^2 2\theta < 0.12(90\%\,\text{CL}) \qquad \text{at } \Delta m^2 \approx 3 \times 10^{-3}\,\text{eV}^2. \tag{8.45}$$

8.6.1.2 Palo Verde

The Palo Verde experiment [Boe01,Bem02] was performed near Phoenix, AZ (USA) and took data from October 1998 to July 2000. The total thermal power of the three reactors used was 11.6 GW and two of them were located 890 m and one 750 m away from the detector. The detector consisted of 12 t of a liquid scintillator also loaded with 0.1% Gd. Because of its rather shallow depth, with a shielding of only about 32 mwe, the detector had to be designed in a modular way. The scintillator was filled in 66 modules, each 9 m long and with $12.7\,\text{cm} \times 25.4$ cm cross section, which were

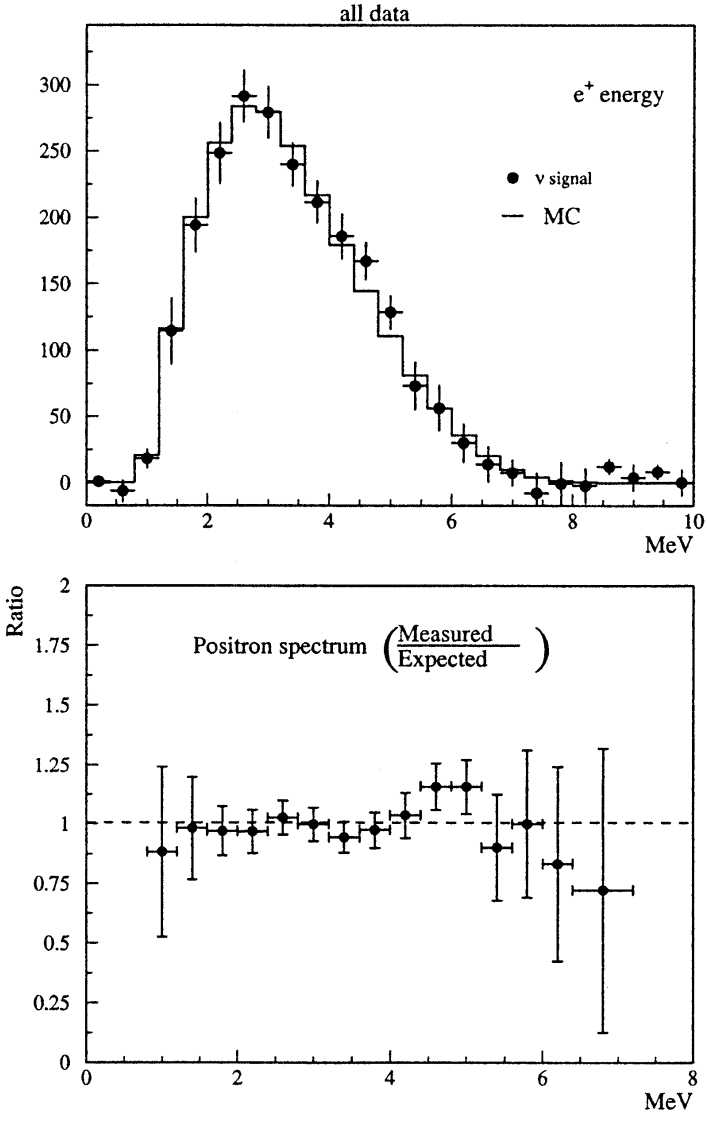

Figure 8.5. Background subtracted positron energy spectrum CHOOZ data. Error bars represent statistical errors only. The filled histogram represent the expectations for the case of no oscillations (from [Apo98]). © 1998 Reprinted with permission from Elsevier.

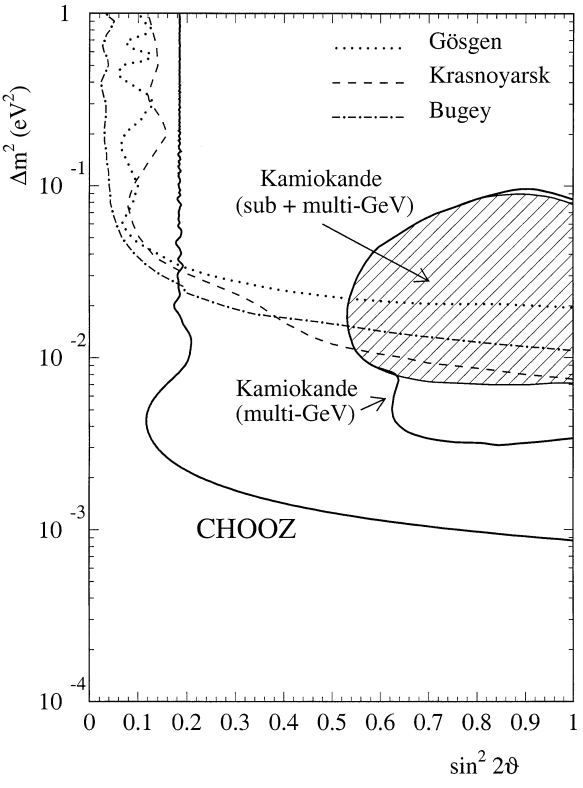

Figure 8.6. Exclusion plot of ν_e–ν_μ oscillations for various reactor experiments. Also shown are the parameter ranges which describe the atmospheric neutrino anomaly (see chapter 9). As can be seen, CHOOZ excludes the ν_e–ν_μ oscillation channel as a possible explanation of the atmospheric neutrino anomaly (from [Apo98]).

arranged in an 11×6 array. The detector was surrounded by a 1m water shield to moderate background neutrons and an additional veto system against cosmic muons using 32 large scintillation counters. The space and time coincidence of three modules coming from two 511 keV photons together with the neutron capture served as a signal.

Also in Palo Verde no evidence for oscillation was seen and a ratio of

$$R = 1.01 \pm 2.4\%(\text{stat.}) \pm 5.3\%(\text{sys.}) \tag{8.46}$$

is given. The resulting exclusion plot is shown in Figure 8.7. Therefore, it can be concluded that ν_μ–ν_e oscillations play only a minor role in the atmospheric neutrino anomaly.

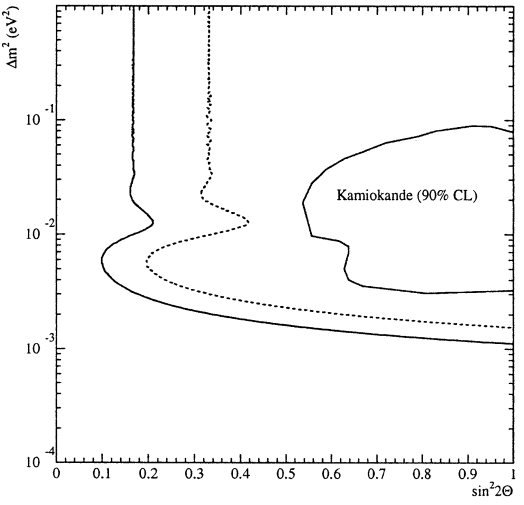

Figure 8.7. Same as figure 8.6 but showing the Palo Verde exlcusion region. The two curves correspond to two different analyses using different background subtraction. The main result here disfavors the ν_e–ν_μ oscillation channel as a possible explanation (from [Boe01]). © 2001 by the American Physical Society.

8.6.1.3 KamLAND

Future activities are motivated by the current solar neutrino data (Chapter 10) implying going to even larger baselines. As discussed in Chapter 10, the preferred solar solution suggests a region of $\Delta m^2 \approx 8 \times 10^{-5}\ \mathrm{eV}^2$ with a large mixing angle $\sin^2 2\theta$. Using (8.24) and the fact that reactor and solar neutrino energies are about the same require a baseline for searches of at least 100 km, two orders of magnitude larger than ever before. The reason this can be done on such short baselines is that here vacuum oscillations are explored and the involved Δm^2 is necessary to produce the matter effects needed for solar neutrinos (see Chapter 10).

An experiment designed for this goal is KamLAND in Japan installed in the Kamioka mine. Taking also reactors from South Korea into account 55 commercial nuclear power plants are delivering a total of 155 GW. Thus, the total flux of $\bar{\nu}_e$ at Kamioka is about $4 \times 10^6\ \mathrm{cm}^{-2}\ \mathrm{s}^{-1}$ (or $1.3 \times 10^6\ \mathrm{cm}^{-2}\ \mathrm{s}^{-1}$ for $E_{\bar{\nu}} > 1.8$ MeV). Of this flux about 70 GW are produced from reactors in a distance of 175 ± 35 km. The detector itself consists of 1000 t of liquid scintillator contained within a sphere. The scintillator is based on mineral oil and pseudocumene, designed to achieve a sufficiently light yield and n–γ discrimination by pulse shape analysis. This inner balloon is surrounded by 2.5 m of non-scintillating fluid as shielding. Both are contained and mechanically supported by a spherical stainless steel vessel. On this vessel 1325 phototubes for readout of the fiducial volume are also mounted. The signal is obtained by a delayed coincidence of the prompt photons from positron annihilation and the 2.2 MeV photons from $\mathrm{p(n,\gamma)d}$ capture.

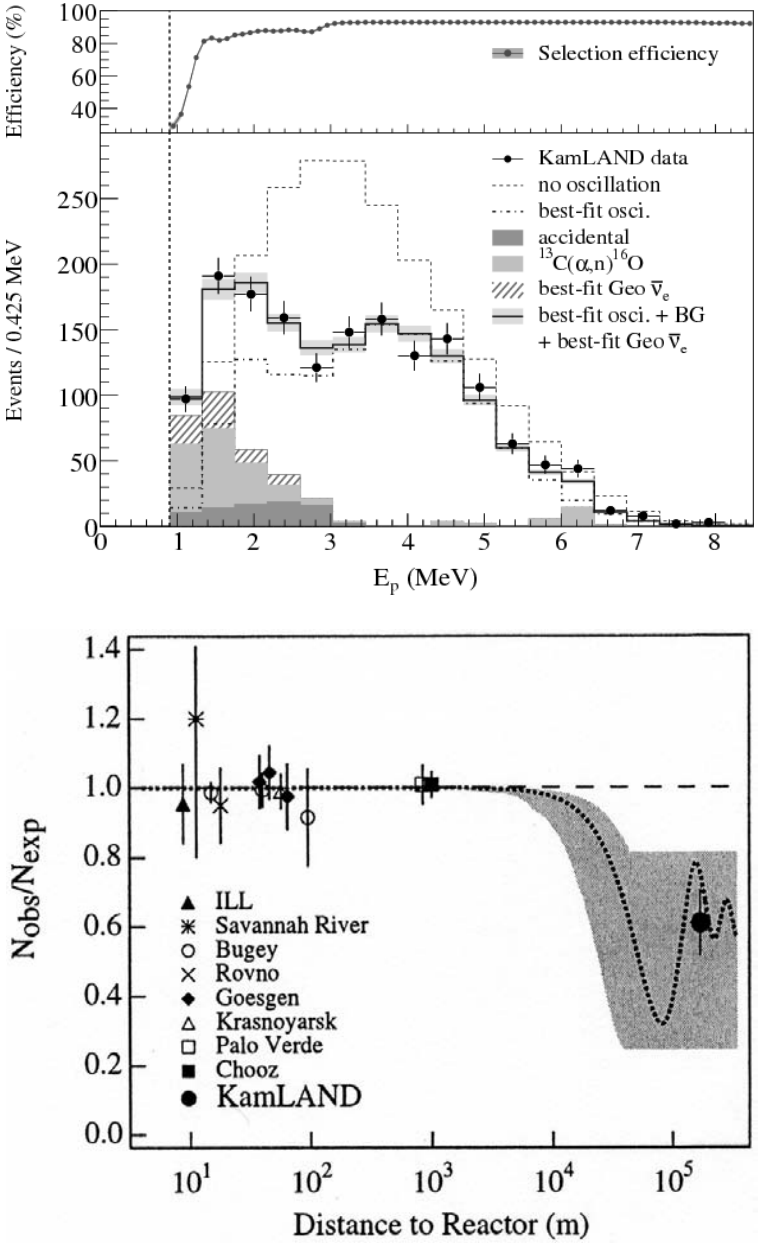

Figure 8.8. Oscillation results from KamLAND. Top: The measured positron spectrum. The deviation from the expected spectral shape can be clearly seen (from [Abe08]). Bottom: Ratio as a function of L/E. A clear reduction with respect to short baseline reactor experiments is seen. For comparison a theoretical oscillation curve is included (from [Egu03]). © 2003 by the American Physical Society.

Impressive results based on three measuring periods have been obtained [Egu03, Ara05, Abe08] with a total exposure of 2881 ton×years. 1609 $\bar{\nu}_e$ events were observed while the expectation had been 2179 ± 89 events (Figure 8.8). The obtained ratio is

$$\frac{N_{\rm obs} - N_{BG}}{N_{\rm exp}} = 0.593 \pm 0.020 \pm 0.026. \tag{8.47}$$

This is clear evidence for neutrino oscillations in form of a ν_e disappearance. The fit parameters are given as

$$\Delta m^2 = 7.58^{+0.21}_{-0.2} \times 10^{-5} eV^2 \quad \text{and} \quad \tan^2\theta = 0.56^{+0.14}_{0.09} \tag{8.48}$$

The implications of this result with respect to the solar neutrino problem will be discussed in Chapter 10. As an exciting byproduct of the oscillation search, for the first time neutrinos from the radioactivity within the Earth have been discovered.

8.6.2 Geoneutrinos

As a remarkable side effect to the reactor neutrino measurements the first detection of geoneutrinos was done by KamLAND [Ara05a]. These are produced by the radioactive beta decays of very long-living isotopes, mainly the ^{238}U, ^{232}Th and ^{235}U decay chains, as well as ^{40}K and ^{87}Rb within the Earth (Figure 8.10). Using the inverse beta decay reaction (8.39) for detection, only ^{238}U and ^{232}Th contributions can be observed. Deeper investigations in the decay chains reveal that in the ^{238}U chain about 88% stem from the beta decay ground state transitions of ^{234m}Pa and ^{214}Bi. In the ^{232}Th chain about 94% of all produced antineutrinos result from ^{212}Bi decay. For a detailled discussion see [Fio07].

Far more uncertain is the distribution of these elements within the Earth, the actual source of heat production within the Earth, and the radiogenic contribution to it. The heat dissipation of the Earth is in the range of 31-44 TW which to certain fraction is supposed to come from these radioactive decays. As a starting point to model the Earth, the Bulk Silicate Earth Model is used [McD99,McD03]. This model links the elemental abundance of the Earth with the one of CI chondritic meteorites due to the common origin in the formation of the solar system. Thus, taking the natural abundance the geoneutrino luminosity L and radiogenic heat production rate H_R can be predicted from the masses of the three elements [Fio07]

$$L = 7.64 \times \mathrm{m(U)} + 1.62 \times \mathrm{m(Th)} + 27.10 \times 10^{-4} \times \mathrm{m(K)} \tag{8.49}$$

$$H_R = 9.85 \times \mathrm{m(U)} + 2.67 \times \mathrm{m(Th)} + 3.33 \times 10^{-4} \times \mathrm{m(K)} \tag{8.50}$$

where units are $10^{24}\mathrm{s}^{-1}$, 10^{12}W and 10^{17}kg, respectively. Out of this model a predicted radiogenic heat production of about 19 TW is predicted. Thus, an antineutrino flux of $\Phi(U,Th) \approx 2 \times 10^6$ cm^{-2}s^{-1} is expected in the same order as the solar ^{8}B neutrino flux. Out of the Bulk Silicate Earth Model various reference geoneutrino models have been created to compare and predict event rates at different locations on the Earth [Man04, Fog05, Eno05]. Experimental locations far from continents have a higher sensitivity to the mantle as the Earth crust is rather thin; the opposite is valid for experiments in the middle of continents.

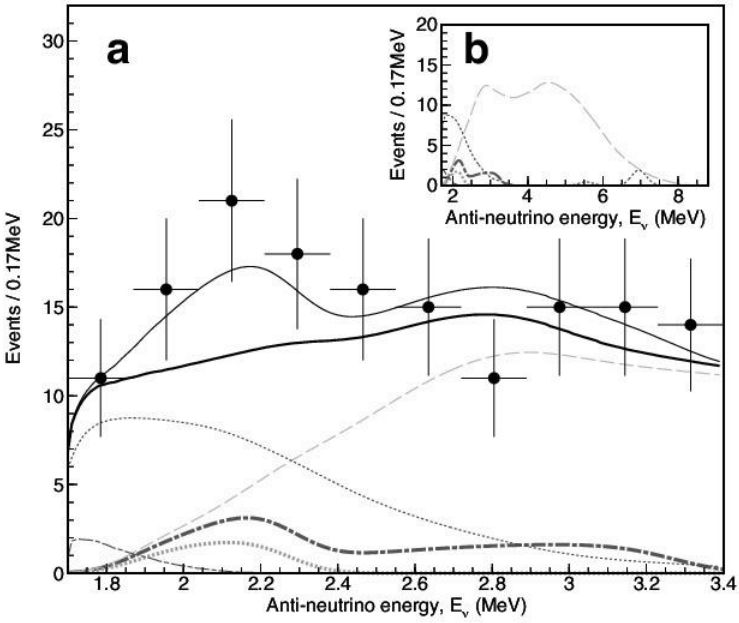

Figure 8.9. Antineutrino energy spectrum as observed by KamLAND. The data points can be fitted (solid line) with five contributions. The dominant ones are reactor antineutrinos (above about 2.3 MeV) and antineutrinos resulting from the $^{13}C(\alpha,n)^{16}O$ reaction (below 2.3 MeV). Additionally two contributions from the U (dash-dotted line) and Th (dotted line) are needed to describe the bump around 2.1 MeV. At very low energy, random coincidences have to be taken into account (from [Ara05a]).

8.6.3 Future

8.6.3.1 Borexino

Another experiment is the solar neutrino experiment Borexino in the Gran Sasso Laboratory described in more detail in Chapter 10, which has started taking data recently. The absence of nuclear power plants in Italy allows a baseline even larger than for KamLAND, typically more than 600 km. However, this implies a lower $\bar{\nu}_e$ flux, and, taking the fact of having only 300 t fiducial volume, a smaller signal is expected. However, on the positive side the lack of reactors might allow for a clean detection of geoneutrinos. The potential for the antineutrino search has been shown with the Counting Test Facility of Borexino [Bal06]. Recently, first geoneutrino events have been detected [Bel10].

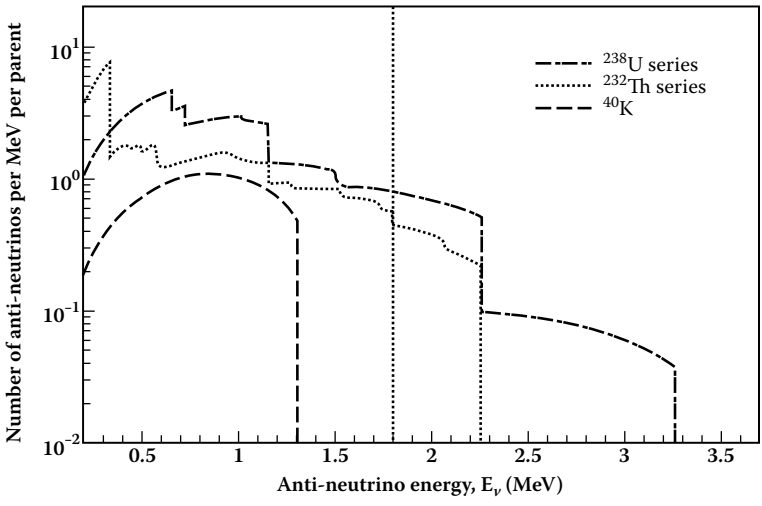

Figure 8.10. Expected geoneutrino energy spectrum from various radioactive sources within the earth. The vertical dotted line corresponds to the energy threshold of inverse beta decay (1.806 MeV). Using this reaction only ^{238}U and ^{232}Th can be observed (with kind permission of S. Enomoto).

8.6.3.2 SNO+

SNO+ is the follow-up experiment of the Sudbury Neutrino Observatory (see Chapter 10). It will be a liquid scintillator detector of KamLAND size but at the depth of SNO. The nearest reactors are about 300 km away and their location fits nicely into the higher minima of the oscillation pattern. This will lead to characteristic "dips" in the observable reactor spectrum and allows a good measurement of geoneutrinos.

8.6.3.3 Measuring θ_{13} at reactors

Within the framework of the next generation experiments, a full 3-flavor analysis of oscillation data including various effects like CP-violation and matter effects must be done. It turns out that the oscillation probably shows a degeneracy among different quantities, which has to be disentangled. An important quantity for future neutrino activities especially within the context of CP violation is the mixing angle θ_{13} as both show up as a product in the Jarlskog invariant (8.22). Its value has to be non-zero to allow a search for CP violation and $\sin^2\theta_{13}$ should be larger than about 0.01 because otherwise there is a drastic change in the CP sensitivity. Reactor experiments provide a clear measurement of θ_{13} by performing disappearance

searches, where the survival probability is given by

$$P(\bar{\nu}_e \to \bar{\nu}_e) \approx 1 - \sin^2\theta_{13}\sin^2\frac{\Delta m^2_{13}L}{4E} - \sin^2\theta_{12}\cos^4\theta_{13}\sin^2\frac{\Delta m^2_{12}L}{4E}. \quad (8.51)$$

To be sensitive enough, a number of nuclear power plants producing a high flux combined with at least two identical detectors (near and far) to observe spectral distortions have to be used as the expected effect is rather small and the systematic error will dominate the result. Various experiments like Double Chooz [Ard06], Daya Bay [Guo07], and Reno [Oh09] are in the building up phase.

8.7 Accelerator-based oscillation experiments

High-energy accelerators offer the chance for both appearance and disappearance searches. Both were and are still commonly used. Having typically much higher beam energies than reactors they probe normally higher Δm^2 regions. However, because of the intensity of the beam, the event rate can be much higher allowing smaller mixing angles $\sin^2 2\theta$ to be probed. Long-baseline ($L \gg 100$ km) experiments are able to extend the accelerator searches down to Δm^2 regions relevant for atmospheric neutrino studies and will be discussed in Chapter 9.

A large number of searches have been performed in the past. Therefore, we will focus on the more recent ones and start with medium-energy experiments, namely LSND, KARMEN, and MiniBooNE.

8.7.1 LSND

The LSND experiment [Ath97] at LANL was a 167 t mineral-oil-based liquid scintillation detector using scintillation and Cerenkov light for detection. It consisted of an approximately cylindrical tank 8.3 m long and 5.7 m in diameter (Figure 8.11). The neutrino beam was produced by a proton beam with 800 MeV kinetic energy hitting a 30-cm long water target located about 1 m upstream of a copper beam stop. The experiment was about 30 m away from the beam stop under an angle of 12° with respect to the proton beam direction and can be called a short-baseline experiment. Most of the π^+ are stopped in the target and decay into muons which come to rest and decay in the target as well. The expected neutrino spectrum has already been shown in Figure 4.28. The decay at rest (DAR) of the positively charged muons allows $\bar{\nu}_\mu \to \bar{\nu}_e$ oscillation to be investigated. A small fraction of the positively charged pions (about 3%) decays in flight in the 1-m long space between target and beam stop and was used for the study of $\nu_\mu \to \nu_e$ oscillations. Note that the beam contamination of $\bar{\nu}_e$ is only of the order 10^{-4} because negative pions are captured by nuclei before decay. LSND took data from 1993 to 1998.

For the DAR analysis in the channel $\bar{\nu}_\mu \to \bar{\nu}_e$, the signal reaction was

$$\bar{\nu}_e + \mathrm{p} \to \mathrm{e}^+ + \mathrm{n}. \quad (8.52)$$

As experimental signature, a positron within the energy range $20 < E_e < 60$ MeV together with a time- and spatial-correlated delayed 2.2 MeV photon from $\mathrm{p(n,\gamma)d}$

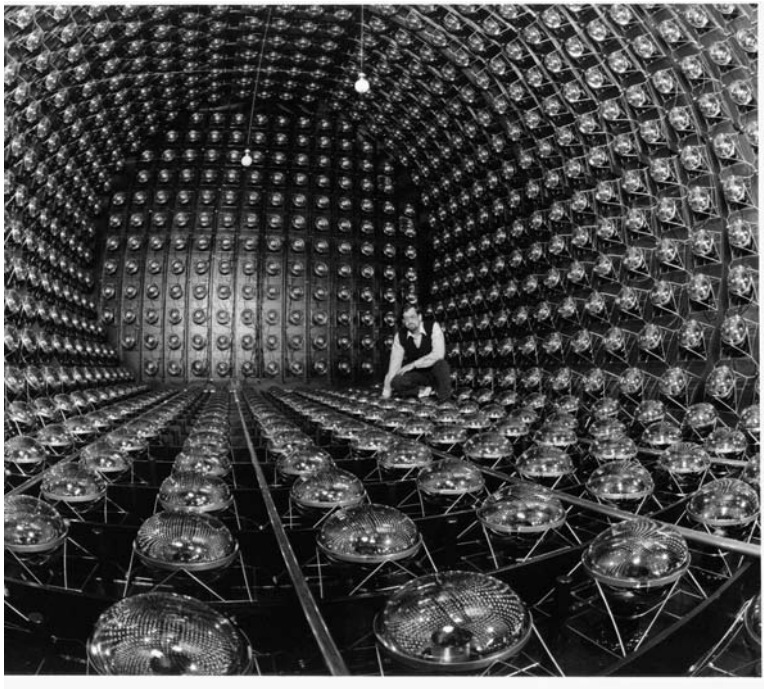

Figure 8.11. Photograph of the interior of the LSND detector (with kind permission of the LSND collaboration).

are required. LSND is not able to distinguish between positron and electron. After background subtraction an excess of $87.9 \pm 22.4 \pm 6.0$ events was indeed observed (Figure 8.10) [Agu01]. Interpreting these as oscillations would correspond to a transition probability of $P(\bar{\nu}_\mu \to \bar{\nu}_e) = 2.64 \pm 0.67 \pm 0.45 \times 10^{-3}$. The analysis, therefore, ends up as evidence for oscillations in the region shown in Figure 8.11.

The DIF analysis is looking for isolated electrons in the region $60 < E_e < 200$ MeV coming from ${}^{12}\mathrm{C}(\nu_e, \mathrm{e}^-)\,{}^{12}\mathrm{N}_{gs}$ reactions. The lower bound of 60 MeV is well above 52.8 MeV, the endpoint of the electron spectrum from muon decay at rest. Here, a total excess of $8.1 \pm 12.2 \pm 1.7$ events was observed showing no clear effect of oscillations [Ath98].

8.7.2 KARMEN

The KARMEN experiment [Dre94] was operated at the neutron spallation source ISIS at Rutherford Appleton Laboratory from 1990 to 2001. KARMEN also used a 800 MeV proton beam but took advantage of the time structure of the beam. It was a pulsed beam having a repetition rate of 50 Hz and consisted of two pulses of 100 ns each with a separation of 325 ns. This time structure of the neutrino beam was important for identifying neutrino-induced reactions and an effective suppression of

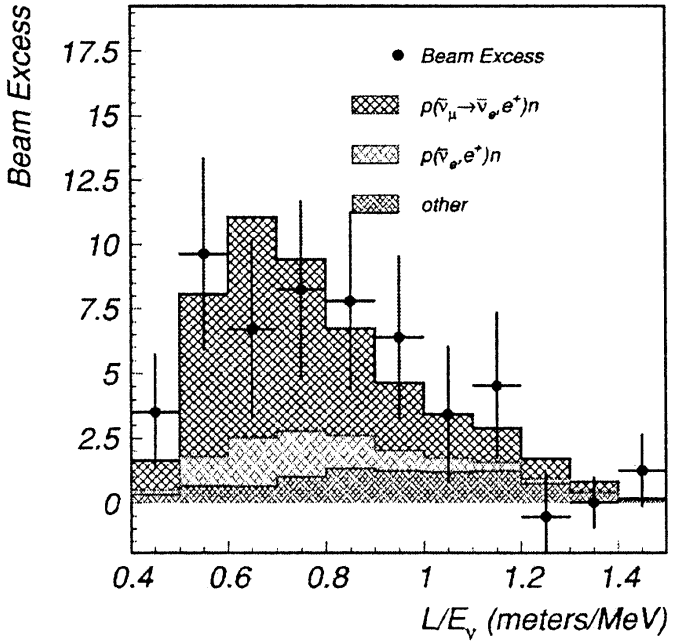

Figure 8.12. The L/E distribution for events with $20 < E_e < 60$ MeV. The data (points) as well as two background components and a fit accounting for the oscillation (hatched area) are shown (from [Agu01]). © 2001 by the American Physical Society.

the cosmic-ray background. The spectral shape of the neutrino beam is identical to the one described for LSND DAR. The detector was installed 18 m away from the target. In order to improve the sensitivity to oscillations by reducing the neutron background, an additional veto shield against atmospheric muons was constructed in 1996 which has been in operation since February 1997 (KARMEN2) and which surrounded the whole detector. The total shielding consisted of 7000 t steel and a system of two layers of active veto counters. The detector itself consisted of 56 t of liquid scintillator. The central scintillation calorimeter was segmented into 512 optically individual modules. The neutron capture detection was done with Gd_2O_3-coated paper within the module walls.

The $\bar{\nu}_\mu \rightarrow \bar{\nu}_e$ analysis again used reaction (8.48). Because of the pulsed beam, positrons were expected within a few μs after beam on target. The signature for detection is a spatially correlated delayed coincidence of a positron with energy up to 51 MeV together with γ-emission from either $\mathrm{p(n,\gamma)d}$ or $\mathrm{Gd(n,\gamma)Gd}$ reactions. The first one results in 2.2 MeV photons while the latter results in photons with a total energy of 8 MeV. The time difference between annihilation and neutron capture is given by thermalization, diffusion and capture of neutrons and is about 110 μs. After analysis of the 1997–2001 dataset, 15 candidates remain with a total expected background of 15.8 events [Arm02]. There is no visible evidence for oscillation and

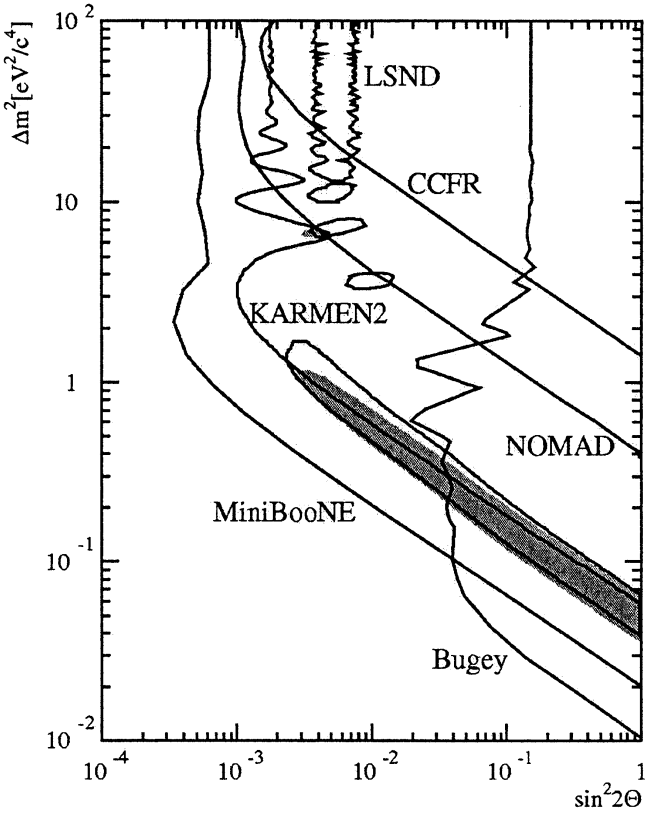

Figure 8.13. Δm^2 *versus* $\sin^2 2\theta$ plot for ν_e–ν_μ oscillations. The parameter ranges describing the LSND evidence as well as the exclusion curves of KARMEN, NOMAD, CCFR and the Bugey reactor experiment are shown (from [Ast03]). © Reprinted with permission from Elsevier.

the excluded region is shown in Figure 8.11 with limits given as $\sin^2 2\theta < 1.7 \times 10^{-3}$ for $\Delta m^2 > 100$ eV^2. Obviously, in the large Δm^2 region ($\Delta m^2 > 10$ eV^2) both experiments are not in agreement; however, in the low-energy region there is still some allowed parameter space for LSND which is not covered by KARMEN. To what extent both experiments are in agreement or not is a severe statistical problem of handling both datasets. Such a combined analysis has been performed [Chu02].

8.7.3 MiniBooNE

The next step to test the full LSND evidence is the MiniBooNE experiment at Fermilab looking for $\nu_\mu \rightarrow \nu_e$ oscillation [Agu09]. The neutrino beam is produced by the Fermilab Booster, sending a high-intensity pulsed proton beam of 8 GeV to a Be target. The positively charged secondaries, mostly pions, are focused by

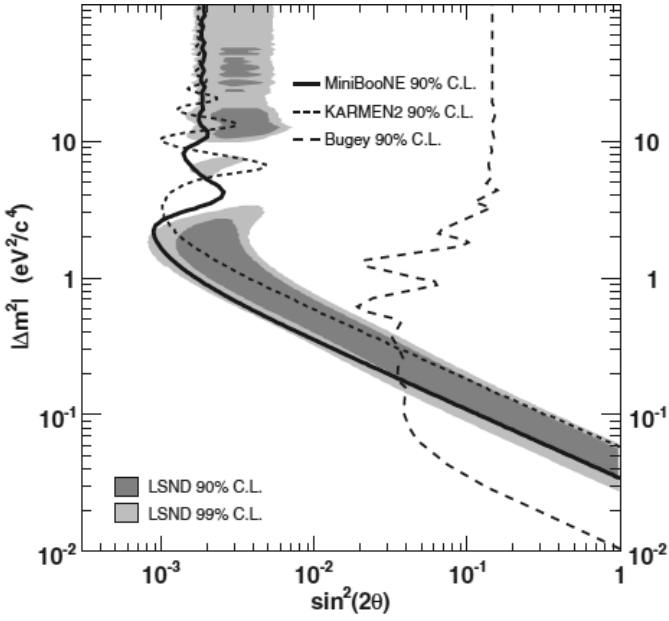

Figure 8.14. Same as figure 8.12 but showing the region of parameters after the MiniBooNE measurement [Agu07]). © 2007 by the American Physical Society.

a magnetic horn and brought into a decay tunnel. This results in an almost pure ν_μ beam (ν_e contamination less than 0.3%). The detector itself is installed about 500 m away from the end of the decay tunnel. It consists of 800 t of pure mineral oil, contained in a 12.2 m diameter spherical tank. A support structure carries about 1550 phototubes for detection of Cerenkov and scintillation light. Data-taking started in August 2002. The data obtained with a ν_μ beam looking for ν_e appearance revealed no evidence for oscillations and excludes most of the parameter space allowed by LSND The result is shown in Figure 8.14 [Agu07]. However, a ν_e excess of events was seen at lower energies which is still unexplained [Agu09c]. To exclude all possible options, in principle the same channel as in LSND has to be explored. This requires a $\bar{\nu}_e$ appearance search in a $\bar{\nu}_\mu$ beam. First results do not show any evidence for an oscillation but due to still low statistics are inconclusive with respect to LSND [Agu09b]. In addition, a recent ν_μ and $\bar{\nu}_\mu$ disappearance search did not show any evidence for oscillations in the Δm^2 region between 0.1-10 eV^2 [Agu09a].

8.8 Searches at higher neutrino energy

Short-baseline oscillation searches were recently performed at higher energies. The main motivation was the search for ν_μ–ν_τ oscillations assuming that ν_τ might have a mass in the eV range and would be a good candidate for hot dark matter (see Chapter 13). The two experiments at CERN performing this search were NOMAD

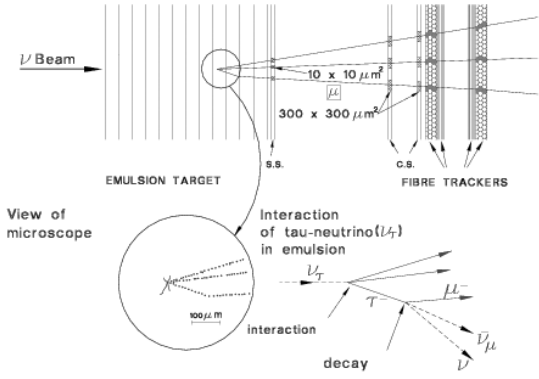

Figure 8.15. ν_τ detection principle used by the CHORUS experiment at CERN. A τ-lepton produced in a CC interaction produces a track of a few hundred μm before its decay. Focusing on the decay into muons the signature results in a kink. The short τ track and the kink are clearly visible because of the excellent spatial resolution of nuclear emulsions.

and CHORUS, both described in more detail in Chapter 4. Therefore, here only the complementary search strategies are discussed.

8.8.1 CHORUS and NOMAD

CHORUS took advantage of the excellent spatial resolution of a few μm of emulsions. The dominant ν_μ beam produced ν_μ CC interactions. An oscillation event would result in a ν_τ CC interaction. Using the average beam energy of about 25 GeV, a produced τ travels about 1 mm before it decays. Such a track is clearly visible in the emulsion and, furthermore, the corresponding kink from the decay can be seen as well (Figure 8.13). After data-taking the emulsions were scanned with automated microscopes equipped with CCD cameras and fast processors. Data were collected from 1994 to 1997 and all 0μ and 1-prong events were analyzed. No signal was found which in the 2-flavor scenario results in an oscillation probability of [Esk01, Esk08]

$$P(\nu_\mu \rightarrow \nu_\tau) \leq 2.2 \times 10^{-4}. \tag{8.53}$$

NOMAD, in contrast, uses kinematical criteria to search for ν_τ. The kinematic situation is shown in Figure 8.15. As can be seen for ν_μ CC, the outgoing lepton is in the plane transverse to the beam more or less back to back to the hadronic final state (momentum conservation) and the missing momentum is rather small. In ν_μ NC events there is large missing momentum and no lepton at about 180 degrees is expected. The signal, namely a ν_τ CC interaction, is somewhere in between. The τ lepton, unlike in CHORUS, is invisible in NOMAD and can only be detected via some of its decay products. They follow the original τ direction resulting in a more back-to-back-like signature. However, in the τ-decay at least one neutrino is produced resulting in significant missing momentum. The analysis now proceeds in a

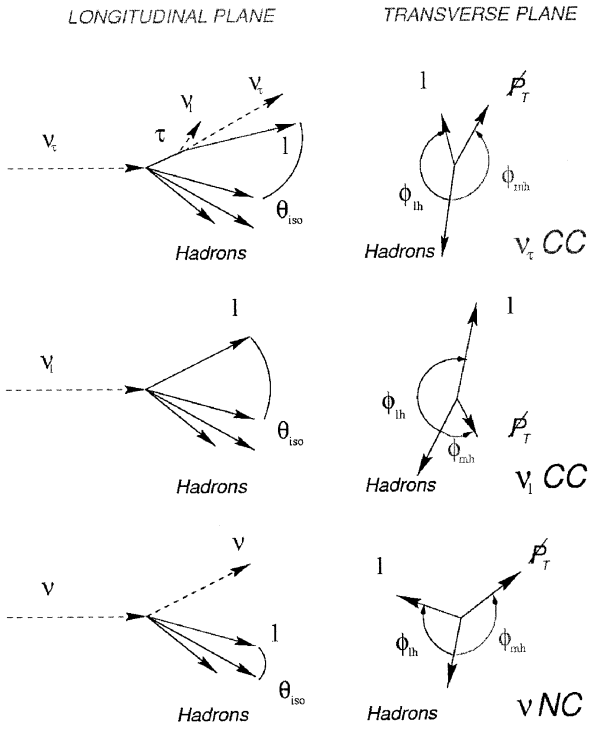

Figure 8.16. ν_τ detection principle used by the NOMAD experiment at CERN. The analysis is based on the kinematics of CC and NC interactions using momentum imbalance and isolation of charged tracks as main criteria because the τ-lepton cannot be observed directly.

way to find optimal experimental variables for the momentum imbalance and lepton isolation to discriminate between these backgrounds and the signal. This is done on the basis of likelihood functions performed as a "blind box" analysis. Also NOMAD did not observe any oscillation signal (55 candidates observed, 58 background events expected) and gives an upper limit for the oscillation probability of [Ast01a]

$$P(\nu_\mu \to \nu_\tau) \leq 2 \times 10^{-4}. \tag{8.54}$$

The exclusion plots of both experiments together with former experiments are shown in Figure 8.17. Using the beam contamination of ν_e, both could also produce limits on $\nu_e \to \nu_\tau$ oscillations [Ast01a]. They are of the order of $P(\nu_e \to \nu_\tau) < 10^{-2}$ and are also shown in Figure 8.17. Recently, NOMAD published their results on ν_e–ν_μ oscillations [Ast03]. Like KARMEN they did not see any evidence and their exclusion curve is also shown in Figure 8.13.

Currently no further short-baseline experiment is planned. One of the reasons is that the atmospheric neutrino anomaly (see Chapter 9) points towards a parameter region of $\Delta m^2 \approx 3 \times 10^{-3}$ eV^2 and large mixing $\sin^2 2\theta \approx 1$. Taking a 1 GeV

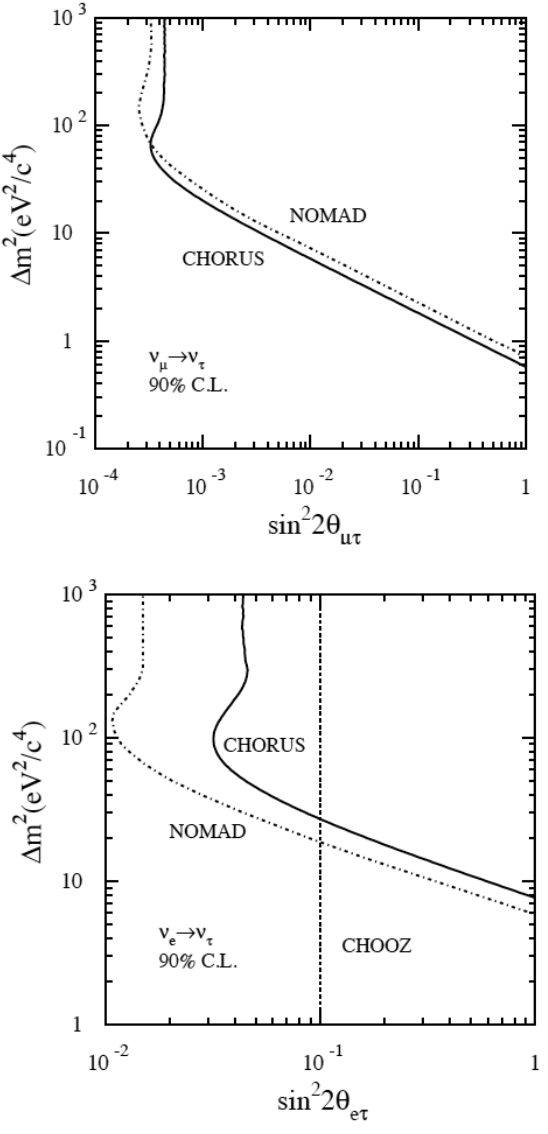

Figure 8.17. Top: ν_μ–ν_τ exclusion plot with the final result of NOMAD and the current result of CHORUS. Both experiments led to an improvement to about one order of magnitude with respect to the former E531 and CCFR experiments at Fermilab. Bottom: ν_e–ν_τ exclusion plot showing the NOMAD and CHORUS result. This is based on the impurity of the used beam containing about 1% ν_e. Also shown is the CHOOZ limit. Note the different Δm^2 region in comparison with Figure 8.6 (from [Esk08]). © 2008 Reprinted with permission from Elsevier.

Table 8.2. The list of matter densities relevant for two-neutrino oscillations.

	$\nu_e \to \nu_{\mu,\tau}$	$\nu_e \to \nu_s$	$\nu_\mu \to \nu_\tau$	$\nu_{\mu,\tau} \to \nu_s$
$\frac{A}{2\sqrt{2}EG_F}$	N_e	$N_e - \frac{1}{2}N_n$	0	$-\frac{1}{2}N_n$

beam this would correspond to an oscillation length of about 500 km, which requires long-baseline experiments. These will be discussed in Chapter 9. Such beams have to cross a significant amount of matter on their way through the Earth and now we want to discuss how matter, in general, might affect neutrino oscillations. This must be taken into account as the determination of the PMNS matrix requires a 3-flavor analysis and the effect will be seen in very long baseline experiments. It is not only of importance for long-baseline experiments, which will be discussed in the next chapter, but also for solar and supernova neutrinos as well.

8.9 Neutrino oscillations in matter

Matter effects can occur if the neutrinos under consideration experience different interactions by passing through matter. In the Sun and the Earth ν_e can have NC and CC interactions with leptons because of the existence of electrons, while for ν_μ and ν_τ only NC reactions are possible. In addition, for a ν_μ beam traversing the Earth, in the case of the existence of sterile neutrinos ν_S, there is a difference between weak reactions (ν_μ) and no weak interactions at all (ν_S), see also [Kuo89, Kim93, Sch97, Bil99].

Starting from the weak interaction Lagrangian (3.48) one gets for low-energy neutrino interactions of flavor ℓ with the background matter

$$-\mathcal{L}_{\nu_\ell} = \frac{G_F}{\sqrt{2}}\nu_\ell^\dagger(1-\gamma_5)\nu_\ell \sum_f N_f(\delta_{\ell f} + I_{3f_L} - 2\sin^2\theta_W Q_f) \tag{8.55}$$

where G_F is the Fermi coupling constant, θ_W the Weinberg angle, I_{3f_L} the eigenvalue of the fermion field f_L of the third component of the weak isospin and Q_f is the charge of f. In the matter Lagrangian (8.55), the CC interaction is represented by the Kronecker symbol $\delta_{\ell f}$ which states that for neutrinos of flavor ℓ the charged current contributes only if background matter containing charged leptons of the same flavor is present. For real matter with electrons, protons and neutrons which is electrically neutral, i.e., $N_e = N_p$, we have $I_{3e_L} = -T_{3p_L} = I_{3n_L} = -1/2$ and $Q_e = -Q_p = -1$, $Q_n = 0$ for electrons, protons and neutrons, respectively. To discuss two-neutrino oscillations in matter two useful definitions are:

$$N(\nu_\alpha) \equiv \delta_{\alpha e}N_e - \tfrac{1}{2}N_n \qquad (\alpha \equiv e,\mu,\tau) \qquad N(\nu_s) \equiv 0 \tag{8.56}$$

following directly from (8.55) and

$$A \equiv 2\sqrt{2}G_F E(N(\nu_\alpha) - N(\nu_\beta)). \tag{8.57}$$

The list of all possible matter densities which determine A and occur in the different oscillation channels is given in Table 8.2. We start with the vacuum case again. The time dependence of mass eigenstates is given by (8.4). Neglecting the common phase by differentiation, we obtain the equation of motion (Schrödinger equation)

$$\mathrm{i}\frac{\mathrm{d}\nu_i(t)}{\mathrm{d}t} = \frac{m_i^2}{2E}\nu_i(t) \tag{8.58}$$

which can be written in matrix notation as follows:

$$\mathrm{i}\frac{\mathrm{d}\nu(t)}{\mathrm{d}t} = H^i\nu(t)$$

with

$$\nu = \begin{pmatrix} \nu_1 \\ . \\ . \\ . \\ \nu_n \end{pmatrix} \tag{8.59}$$

and

$$H^i_{ij} = \frac{m_i^2}{2E}\delta_{ij}.$$

H^i is the Hamilton matrix ('mass matrix') in the ν_i representation and it is diagonal, i.e., the mass eigenstates in vacuum are eigenstates of H. By applying the unitary transformation

$$\nu = U^\dagger\nu' \qquad \text{with } \nu' = \begin{pmatrix} \nu_\alpha \\ . \\ . \\ . \end{pmatrix} \tag{8.60}$$

and the mixing matrix U, the equation of motion and the Hamilton matrix H^α can be written in the representation of flavor eigenstates ν_α:

$$\mathrm{i}\frac{\mathrm{d}\nu'(t)}{\mathrm{d}t} = H^\alpha\nu'(t) \qquad \text{with } H^\alpha = UH^iU^\dagger. \tag{8.61}$$

Consider the case of two neutrinos (ν_e, ν_μ): the Hamilton matrix can be written in both representations as

$$\begin{aligned} H^i &= \frac{1}{2E}\begin{pmatrix} m_1^2 & 0 \\ 0 & m_2^2 \end{pmatrix} \\ H^\alpha &= \frac{1}{2E}\begin{pmatrix} m_{ee}^2 & m_{e\mu}^2 \\ m_{e\mu}^2 & m_{\mu\mu}^2 \end{pmatrix} \\ &= \frac{1}{2E}\begin{pmatrix} m_1^2\cos^2\theta + m_2^2\sin^2\theta & (m_2^2 - m_1^2)\sin\theta\cos\theta \\ (m_2^2 - m_1^2)\sin\theta\cos\theta & m_1^2\sin^2\theta + m_2^2\cos^2\theta \end{pmatrix} \\ &= \frac{1}{4E}\Sigma\begin{pmatrix} 1 & 0 \\ 0 & 1 \end{pmatrix} + \frac{1}{4E}\Delta m^2\begin{pmatrix} -\cos 2\theta & \sin 2\theta \\ \sin 2\theta & \cos 2\theta \end{pmatrix} \end{aligned} \tag{8.62}$$

with $\Sigma = m_2^2 + m_1^2$ and $\Delta m^2 = m_2^2 - m_1^2$. How does the behavior change in matter? As already stated, the ν_e mass is modified in matter according to (using ν_e and ν_μ as examples)

$$m_{ee}^2 \to m_{eem}^2 = m_{ee}^2 + A \qquad \text{with } A = 2\sqrt{2} G_F E N_e \tag{8.63}$$

the latter following directly from (8.57). The Hamilton matrix H_m^α in matter is, therefore, given in the flavor representation as

$$\begin{aligned} H_m^\alpha &= H^\alpha + \frac{1}{2E}\begin{pmatrix} A & 0 \\ 0 & 0 \end{pmatrix} = \frac{1}{2E}\begin{pmatrix} m_{ee}^2 + A & m_{e\mu}^2 \\ m_{e\mu}^2 & m_{\mu\mu}^2 \end{pmatrix} \\ &= \frac{1}{4E}(\Sigma + A)\begin{pmatrix} 1 & 0 \\ 0 & 1 \end{pmatrix} \\ &\quad + \frac{1}{4E}\begin{pmatrix} A - \Delta m^2 \cos 2\theta & \Delta m^2 \sin 2\theta \\ \Delta m^2 \sin 2\theta & -A + \Delta m^2 \cos 2\theta \end{pmatrix}. \end{aligned} \tag{8.64}$$

The same relations hold for antineutrinos with the exchange $A \to -A$. Transforming this matrix back into the (ν_1, ν_2) representation results in

$$\begin{aligned} H_m^i = U^\dagger H_m^\alpha U &= U^\dagger H^\alpha U + \frac{1}{2E} U^\dagger \begin{pmatrix} A & 0 \\ 0 & 0 \end{pmatrix} U \\ &= H^i + \frac{1}{2E} U^\dagger \begin{pmatrix} A & 0 \\ 0 & 0 \end{pmatrix} U \\ &= \frac{1}{2E}\begin{pmatrix} m_1^2 + A\cos^2\theta & A\cos\theta\sin\theta \\ A\cos\theta\sin\theta & m_2^2 + A\sin^2\theta \end{pmatrix}. \end{aligned} \tag{8.65}$$

The matrix now contains nondiagonal terms, meaning that the mass eigenstates of the vacuum are no longer eigenstates in matter. To obtain the mass eigenstates (ν_{1m}, ν_{2m}) in matter and the corresponding mass eigenvalues (m_{1m}^2, m_{2m}^2) (effective masses) H_m^i must be diagonalized. This results in mass eigenstates of

$$m_{1m,2m}^2 = \frac{1}{2}\left[(\Sigma + A) \mp \sqrt{(A - \Delta m^2 \cos 2\theta)^2 + (\Delta m^2)^2 \sin^2 2\theta}\right]. \tag{8.66}$$

For $A \to 0$, it follows that $m_{1m,2m}^2 \to m_{1,2}^2$. Considering now a mixing matrix U_m connecting the mass eigenstates in matter $m_{1m,2m}$ with the flavor eigenstates (ν_e, ν_μ) the corresponding mixing angle θ_m is given by

$$\begin{aligned} \tan 2\theta_m &= \frac{\sin 2\theta}{\cos 2\theta - A/\Delta m^2} \\ \sin 2\theta_m &= \frac{\sin 2\theta}{\sqrt{(A/\Delta m^2 - \cos 2\theta)^2 + \sin^2 2\theta}}. \end{aligned} \tag{8.67}$$

Here again, for $A \to 0$, it follows that $\theta_m \to \theta$. Using the relation

$$\Delta m_m^2 = m_{2m}^2 - m_{1m}^2 = \Delta m^2 \sqrt{\left(\frac{A}{\Delta m^2} - \cos 2\theta\right)^2 + \sin^2 2\theta} \tag{8.68}$$

the oscillation probabilities in matter can be written analogously to those of the vacuum:

$$P_m(\nu_e \to \nu_\mu) = \sin^2 2\theta_m \times \sin^2 \frac{\Delta m_m^2}{4} \times \frac{L}{E} \tag{8.69}$$

$$P_m(\nu_e \to \nu_e) = 1 - P_m(\nu_e \to \nu_\mu) \tag{8.70}$$

with a corresponding oscillation length in matter:

$$L_m = \frac{4\pi E}{\Delta m_m^2} = \frac{L_0}{\sqrt{\left(\frac{A}{\Delta m^2} - \cos 2\theta\right)^2 + \sin^2 2\theta}} = \frac{\sin 2\theta_m}{\sin 2\theta} L_0. \tag{8.71}$$

Note already here that (8.64) allows the possibility of maximal mixing in matter, $\sin 2\theta_m \approx 1$, even for small $\sin\theta$ because of the resonance type form.

8.10 Future activities—Determination of the PMNS matrix elements

Having established neutrino oscillations, one of the major goals now is to determine the PMNS matrix elements more precisely and search for a possible CP-violation in the lepton sector. Obviously, this requires a full 3-flavor analysis of all the available data. The expressions for the 3-flavor oscillation probabilities including matter effects are quite complex, as an example P($\nu_\mu \to \nu_e$) can be expressed as

$$P(\nu_\mu \to \nu_e) = P_1 + P_2 + P_3 + P_4 \tag{8.72}$$

with

$$P_1 = \sin^2\theta_{23} \sin^2 2\theta_{13} (\frac{\Delta_{13}}{B_\pm})^2 \sin^2 \frac{B_\pm L}{2} \tag{8.73}$$

$$P_2 = \cos^2\theta_{23} \sin^2 2\theta_{12} (\frac{\Delta_{12}}{A})^2 \sin^2 \frac{AL}{2} \tag{8.74}$$

$$P_3 = J \cos\delta (\frac{\Delta_{13}}{B_\pm})(\frac{\Delta_{12}}{A}) \cos\frac{\Delta_{13} L}{2} \sin\frac{AL}{2} \sin\frac{B_\pm L}{2} \tag{8.75}$$

$$P_4 = \mp J \sin\delta (\frac{\Delta_{13}}{B_\pm})(\frac{\Delta_{12}}{A}) \cos\frac{\Delta_{13} L}{2} \sin\frac{AL}{2} \sin\frac{B_\pm L}{2} \tag{8.76}$$

with $\Delta_{ij} = \Delta m_{ij}^2/(2E)$, $A = \sqrt{2} G_F n_e, B_\pm = \mid A \pm \Delta_{13} \mid$ and $J = \cos\theta_{13} \sin 2\theta_{12} \sin 2\theta_{13} \sin 2\theta_{23}$. The +(-) sign is for neutrinos (antineutrinos). Thus, the three angles and one phase in the PMNS matrix have to be measured with higher accuracies. One of the ultimate goals is to investigate CP-violation in the lepton sector. As in the quark sector, the CP-phase is always part of a product with all mixing angles, the Jarlskog-invariant J (see (8.22)), hence always with the still badly known angle θ_{13}. An additional problem arises in the form of parameter degeneracy. Assuming that all mixing parameters except θ_{13} and δ are known, and

a precise measurement of $P(\nu_\mu \rightarrow \nu_e)$ and $P(\bar{\nu}_\mu \rightarrow \bar{\nu}_e)$ has been performed, there is still a situation where you find four different solutions (two for CP-even, two for CP-odd) [Bur01, Bar02]. The only chance to remove the ambiguities is to perform either an experiment at two different energies or baselines or to combine two different experiments. In matter, the measurement of CP violation can become more complicated because the oscillation probabilities for neutrinos and antineutrinos are, in general, different in matter, even if $\delta = 0$. Indeed, the matter effect can either contaminate or enhance the effect of an intrinsic CP violation effect coming from δ [Ara97, Min98, Min00, Min02]. For the case of T violation, the situation is different. If $\Delta P^T_{\alpha\beta} \neq 0$ for $\alpha \neq \beta$ would be established, then this implies $\delta \neq 0$ even in the presence of matter. The reason is that the oscillation probability is invariant under time reversal even in the presence of matter. Similar to the case of CP violation, T violation effects can either be enhanced or suppressed in matter [Par01]. However, a measurement of T violation is experimentally more difficult to perform because there is a need for a non-muon neutrino beam, like a beta beam. Additionally, matter effects also give a handle on the determination of the sign of Δm^2_{23}.

A compilation of expected matter effects and CP violation is shown in Figure 8.18.

To accomplish this physics program a variety of ideas for new beams with very high intensity has been pushed forward. As already mentioned, nuclear reactors provide a clean measurement of θ_{13} without any degeneracy problems.

8.11 Possible future beams

Future accelerator-based activities fall into three catagories, superbeams, beta beams and neutrino factories using a muon storage ring, which will be discussed next.

8.11.1 Off-axis superbeams

Conventional neutrino beams in the GeV range run into systematics when investigating oscillations involving ν_μ and ν_e because of the beam contaminations of ν_e from K_{e3} decays (see Chapter 4). To reduce this component, lower energy beams with high intensity are proposed. Here, quasi-elastic interactions are dominant and it would be convienent to have a narrow band beam. This can be achieved by going off axis and it is due to the pion decay kinematics. The ν_μ momentum in the laboratory frame is given by

$$p_L = \gamma(p^* \cos\theta^* + \beta p^*) \tag{8.77}$$

$$p_T = p^* \sin\theta^* \tag{8.78}$$

with $p^* = 0.03$ GeV/c as the neutrino momentum and θ^* as the polar angle of neutrino emission with respect to the pion direction of flight, both given in the pion rest frame. In the laboratory frame, θ is given by

$$\theta = \frac{R}{L} = \frac{1}{\gamma}\frac{\sin\theta^*}{1+\cos\theta^*} \tag{8.79}$$

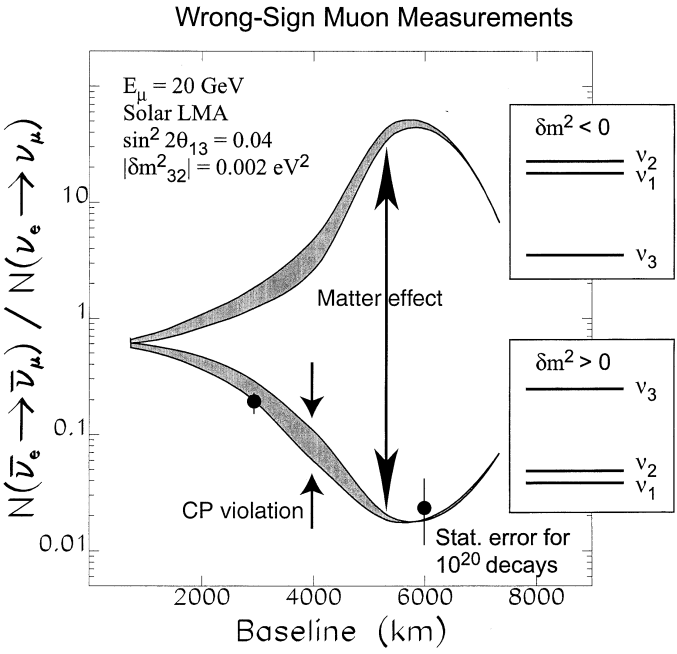

Figure 8.18. Possibilities for observing CP violation and matter effects using beams from a neutrino factory by using wrong sign muons. Matter effects start to significantly split in two bands if a detector is at least 1000 km away from the source. The two bands correspond to normal and inverted mass hierarchies. The width of the band gives the size of the possible CP violation using the parameters stated. It will be observable only if the LMA solution of the solar neutrino problem is correct (see Chapter 10) and if the angle θ_{13} in the MNS matrix is different from zero.

with L as the baseline and R as the distance of the detector from the beam center. If the neutrino emission in the pion rest frame is perpendicular to the pion flight direction ($\theta^* = 90°$), then

$$\theta = \frac{1}{\gamma}. \tag{8.80}$$

The neutrino energy E_ν as a function is given by

$$E_\nu(R) = \frac{2\gamma p^*}{1 + (\gamma R/L)^2} \tag{8.81}$$

which is half of the energy at beam centre for $\theta = 1/\gamma$. However, the most important kinematic property is that, at this angle, the neutrino energy is, in first order, independent of the energy of the parent pion

$$\frac{\partial E_\nu}{\partial \gamma} = 0. \tag{8.82}$$

This opens a way for an NBB with a high intensity. A first realization is the T2K experiment. The newly built Japanese Hadron Facility (JHF) in Tokai is producing a 0.77 MW beam of protons with 50 GeV on a target and using Super-Kamiokande as the far detector being about 2.5 degrees off axis [Aok03]. The baseline corresponds to 295 km. The experiment has started data taking recently. This can be updated in a second phase to 4 MW and also a 1 Mt detector (Hyper-Kamiokande). The future detector might be split in two using a side in Korea instead (T2KK). Also a 100 kt LAr detector is considered. A similar idea exists at CERN to use the proposed superconducting proton linac (SPL) making a high-intensity beam to the Modane Underground Laboratory (130 km away), where the MEMPHYS water Cerenkov detector with a total mass of 435 kt would be installed. A search for θ_{13} in a parasitic mode of already existing beam-lines such as NuMI will also be done with NOνA, about 810 km away from Fermilab. Also the newly planned DUSEL underground facility in the USA is considered for long-baseline experiments. The idea in all experiments is to measure ν_e appearance in a ν_μ beam. The oscillation probability is directly proportional to $\sin^2\theta_{13}$. In addition, such experiments would also allow $\sin^2 2\theta_{23}$ and Δm^2_{23} to be measured.

8.11.2 Beta beams

The idea is to accelerate β-unstable isotopes [Zuc02] to energies of a few 100 MeV using ion accelerators such as ISOLDE at CERN. This would give a clearly defined beam of ν_e or $\bar{\nu}_e$with a maximal neutrino energy of $E_\nu \leq 2\gamma Q$ and a beam opening angle of $\theta \leq 1/\gamma$, with the relativistic factor γ and Q as the transition energy in beta decay (see Chapter 6). Among the favored isotopes discussed are ^{6}He in the case of a $\bar{\nu}_e$ beam and ^{18}Ne in the case of a ν_e beam; see for example [Ter04, Bur05, Vol07].

8.11.3 Muon storage rings—neutrino factories

In recent years the idea to use muon storage rings to obtain high-intensity neutrino beams has become very popular [Gee98, Aut99, Alb00, Als02, Apo02, Ban09]. The two main advantages are the precisely known neutrino beam composition and the high intensity (about 10^{21} muons/yr should be filled in the storage ring). A conceptional design is shown in Figure 8.19. Even if many technical challenges have to be solved, it offers a unique source for future accelerator-based neutrino physics. First experimental steps towards its realization are on their way; among them are the HARP experiment at CERN, which determines the target for optimal production of secondaries, the study of muon scattering (MUSCAT experiment) and muon cooling (MICE experiment). For additional information see also [Nuf01, Nuf02, Hub02, Gee07, Nuf08, Ban09, Gee09].

Muon decay as neutrino source provides $\nu_e(\bar{\nu}_e)$ and $\bar{\nu}_\mu(\nu_\mu)$as beams simultaneously. Hence, for oscillation searches in the appearance channel for $\nu_e \rightarrow \nu_\mu$the signal will be a wrong-signed muon and thus charge identification is a crucial part of the any detector concept. A compilation of search modes is given in Table 8.3.

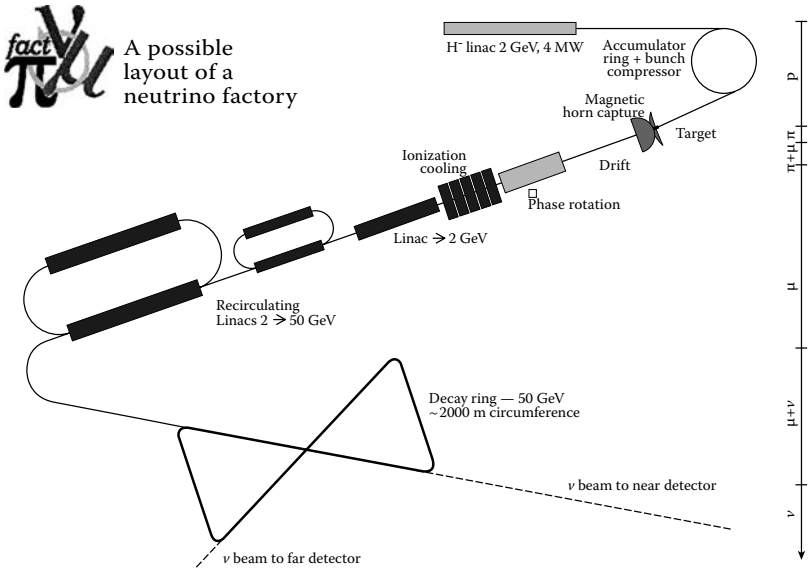

Figure 8.19. Proposed layout for a neutrino factory. The main ingredients are: a high intensity proton linac, a target able to survive the deposited energy and giving a good yield of pions, a cooling device for the decay muons, an accelerator for the muons and a storage ring allowing for muon decay and therefore neutrino beams.

Table 8.3. The various oscillation channels available at a neutrino factory.

$\mu^+ \to e^+ \nu_e \bar{\nu}_\mu$	$\mu^- \to e^- \bar{\nu}_e \nu_\mu$		name
$\bar{\nu}_\mu \to \bar{\nu}_\mu$	$\nu_\mu \to \nu_\mu$	disappearance	
$\bar{\nu}_\mu \to \bar{\nu}_e$	$\nu_\mu \to \nu_e$	appearance	platinum channel
$\bar{\nu}_\mu \to \bar{\nu}_\tau$	$\nu_\mu \to \nu_\tau$	appearance (atm. osc.)	
$\nu_e \to \nu_\mu$	$\bar{\nu}_e \to \bar{\nu}_\mu$	appearance	golden channel
$\nu_e \to \nu_e$	$\bar{\nu}_e \to \bar{\nu}_e$	disappearance	
$\nu_e \to \nu_\tau$	$\bar{\nu}_e \to \bar{\nu}_\tau$	appearance	silver channel

To disentangle the 8-fold degeneracy among the parameters, several of the channels have to be used. Furthermore, a measurement at two different locations from the source and thus at two different values of L/E will help. Alternatively, binned energy spectra for a given distance will work in the same spirit. A special distance for an experiment would be the "magic baseline" L of about 7300–7600 km, because of

$$\sqrt{2} G_F n_e L = \frac{\pi}{2} \to \sin(\frac{AL}{2}) = 0 \tag{8.83}$$

As a consequence only the term P_1 in (8.72) is non-vanishing.

This page intentionally left blank